Molecular Plant • Volume 3 • Number 1 • Pages 78–90 • January 2010 RESEARCH ARTICLE

The Formation of Anthocyanic Vacuolar Inclusions in *Arabidopsis thaliana* and Implications for the Sequestration of Anthocyanin Pigments

Lucille Pourcel[a], Niloufer G. Irani[a,c], Yuhua Lu[a,d], Ken Riedl[b], Steve Schwartz[b] and **Erich Grotewold[a,1]**

a Department of Plant Cellular and Molecular Biology and Plant Biotechnology Center, Ohio State University, Columbus, OH 43210, USA
b Department of Food Science and Technology, The Ohio State University, Columbus, OH 43210, USA
c Present address: Department of Plant Systems Biology, Flanders Institute for Biotechnology, and Department of Plant Biotechnology and Genetics, Ghent University, 9052 Ghent, Belgium
d Current address: Department of Chemistry, Eastern Illinois University, Charleston, IL 61920, USA

ABSTRACT Anthocyanins are flavonoid pigments that accumulate in the large central vacuole of most plants. Inside the vacuole, anthocyanins can be found uniformly distributed or as part of sub-vacuolar pigment bodies, the Anthocyanic Vacuolar Inclusions (AVIs). Using *Arabidopsis* seedlings grown under anthocyanin-inductive conditions as a model to understand how AVIs are formed, we show here that the accumulation of AVIs strongly correlates with the formation of cyanidin 3-glucoside (C3G) and derivatives. *Arabidopsis* mutants that fail to glycosylate anthocyanidins at the 5-*O* position (*5gt* mutant) accumulate AVIs in almost every epidermal cell of the cotyledons, as compared to wild-type seedlings, where only a small fraction of the cells show AVIs. A similar phenomenon is observed when seedlings are treated with vanadate. Highlighting a role for autophagy in the formation of the AVIs, we show that various mutants that interfere with the autophagic process (*atg* mutants) display lower numbers of AVIs, in addition to a reduced accumulation of anthocyanins. Interestingly, vanadate increases the numbers of AVIs in the *atg* mutants, suggesting that several pathways might participate in AVI formation. Taken together, our results suggest novel mechanisms for the formation of sub-vacuolar compartments capable of accumulating anthocyanin pigments.

Key words: Anthocyanin; autophagy; cyanidin 3-glucoside; vacuolar inclusion; vanadate.

INTRODUCTION

Plants accumulate large numbers of 'specialized' compounds (a.k.a. natural products, phytochemicals) that need to be properly transported and stored until used. In sharp contrast to our exceptional understanding of plant metabolism and metabolic pathways (Buchanan et al., 2000), little continues to be known on the mechanisms used by plants to transport and sequester specialized compounds. This is likely to hinder future efforts to rationally manipulate plant metabolic pathways.

Anthocyanins are one of the major classes of plant pigments, which serve multiple eco-physiological functions, including providing visual clues to pollinators and seed dispersers (Grotewold, 2006), and protecting plants from various stress conditions (Gould, 2004). Anthocyanidins, corresponding to anthocyanin aglycones, are synthesized from the general phenylpropanoid pathway, by the action of several flavonoid biosynthetic enzymes loosely associated with the cytoplasmic face of the endoplasmic reticulum (ER) (Winkel, 2004; Winkel-Shirley, 1999).

[1] To whom correspondence should be addressed. E-mail grotewold.1@osu.edu, fax (614) 292-5379, tel. (614) 292-2483.

doi: 10.1093/mp/ssp071, Advance Access publication 28 August 2009
Received 5 May 2009; accepted 28 July 2009

Anthocyanidins are subjected to multiple modifications that include glycosylation, methylation, and acylation (Winkel, 2008). In *Arabidopsis*, anthocyanidins can be glycosylated at the 3-*O* and/or 5-*O* positions by the corresponding UDP-glucose:flavonoid 3-*O*-glucosyltransferase (3GT, At5g17050) and UDP-glucose:cyanidin 5-*O*-glucosyltransferase (5GT, At4g14090) enzymes (Tohge et al., 2005), respectively. Once synthesized, anthocyanins accumulate in a large central vacuole, this localization being necessary to prevent oxidation (Marrs et al., 1995) and for anthocyanins to function as pigments in the acidic vacuolar pH (Verweij et al., 2008), or to be stored until further use. Thus, anthocyanins or their precursors need to be transported from the cytoplasmic surface of the ER to the vacuole. Two non-exclusive possible models for the transport of anthocyanins to the vacuole have been proposed: the Ligandin Transporter (LT) and the Vesicular Transport (VT) models (Grotewold and Davis, 2008). The LT model is largely based on the observation that mutations in some glutathione *S*-transferases (GSTs) genes, such as the maize *BZ2* (Marrs et al., 1995), Petunia *AN9* (Mueller et al., 2000), and *Arabidopsis TT19* (Kitamura et al., 2004) genes, prevent the vacuolar localization of anthocyanins. Interestingly, the GST enzymatic activity is not required for the GST-dependent anthocyanin vacuolar sequestration, resulting in the suggestion that these GSTs serve as 'ligandins', necessary for escorting anthocyanins, such as cyanidin 3-*O*-glucoside (C3G), from the ER to the tonoplast (Mueller et al., 2000). Tonoplast transporters, such as maize MRP3 (Goodman et al., 2004), would recognize the GST–C3G complex and pump C3G into the vacuole. The VT model is based on the observation that in many plants, anthocyanins and other flavonoids accumulate in the cytoplasm in discrete structures (Grotewold et al., 1998; Hsieh and Huang, 2007; Nozue and Yasuda, 1985; Poustka et al., 2007; Small and Pecket, 1980; Small and Pecket, 1982; Zhang et al., 2006). Consistent with this model, in *Arabidopsis*, anthocyanins have recently been shown to first accumulate in the ER lumen. From the ER, one pathway for anthocyanin transport to the vacuole involves vesicles marked by GFP–Chi, corresponding to a fusion of the green fluorescent protein (GFP) to the C-terminal vacuolar sorting determinant (VSD) from the barley chitinase A protein, normally targeted to the large central vacuole directly from the ER (Poustka et al., 2007).

Once inside the vacuole, anthocyanins are sometimes found uniformly distributed in the lumen. However, in a large number of plant species, anthocyanins accumulate in discrete subvacuolar structures called by a number of names that reflect their diversity (Grotewold and Davis, 2008). Anthocyanoplasts have been described for many plants as spherical intravacuolar membrane-bound structures (Pecket and Small, 1980). In seedlings of red radish and *Prunus* callus, anthocyanoplasts are first visualized as cytoplasmic membranous vesicles packed with anthocyanin pigments, which then fuse to yield large anthocyanin-containing bodies (Nozzolillo and Ishikura, 1988). These structures resemble very much what we observed in Maize Black Mexican Sweet (BMS) cells expressing the C1 and R regulators of anthocyanin biosynthesis (Grotewold et al., 1998; Irani and Grotewold, 2005). In contrast, the 'intravacuolar pigmented globules' (cyanoplasts) present in sweet potato cells appear as membrane-less (Nozue et al., 1993), and their formation requires the VP24 metalloprotease, which co-localizes with the pigments (Nozue et al., 2003, 1997; Xu et al., 2000, 2001). Similar structures, the AVIs (anthocyanic vacuolar inclusions), have been identified in a number of plants (Markham et al., 2000). *Arabidopsis* seedlings and plants induced to accumulate large quantities of anthocyanins also show AVI-like structures. Resembling the neutral red (NR) staining 'intravacuolar spherical bodies' of *Polygonum cupsidatum* (Japanese knotweed), which exist inside the vacuole even in the absence of anthocyanins, and which get filled when pigment formation is induced (Kubo et al., 1995), *Arabidopsis* mutants deficient in anthocyanin accumulation harbor NR-staining sub-vacuolar structures that increase in number and accumulate pigment upon anthocyanin induction (Poustka et al., 2007). In grapevine suspension cultures, AVIs selectively accumulate acylated anthocyanins (Conn et al., 2003), suggesting that perhaps AVIs serve a specific role in aggregating or sequestering anthocyanins with particular modifications.

The mechanisms by which anthocyanins and other flavonoids are imported into the vacuole remain unclear. It is possible that tonoplast-localized ZmMRP3-like (Goodman et al., 2004) or Multidrug and Toxic Compound Extrusion (MATE) transporters, such as *Arabidopsis* TT12 (Debeaujon et al., 2001; Marinova et al., 2007), participate in the uptake of cytoplasmic anthocyanins. However, it is difficult to imagine how tonoplast-localized transporters might negotiate the uptake of anthocyanins sequestered inside vesicles. Autophagy is involved in vacuole biogenesis (Marty, 1999; Moriyasu and Hillmer, 2000) and the formation of protein bodies in the aleurones of cereals involves at least two possible autophagic pathways (reviewed in Moriyasu and Hillmer, 2000). Thus, it is conceivable that anthocyanin-containing ER-derived vesicles might be taken up by the vacuole via an autophagic mechanism. A number of *Arabidopsis* proteins required for autophagy have been described, and increasing evidence suggests a role for autophagy in cellular processes other than in response to starvation (reviewed in Bassham, 2007).

Here, we investigated the formation of AVIs in several mutants and under various conditions in *Arabidopsis*. The accumulation of AVIs strongly correlates with the formation of cyanidin 3-*O*-glucoside (C3G) and its derivatives. *Arabidopsis* mutants that fail to glycosylate anthocyanidins at the 5-*O* position (*5gt* mutant) form AVIs in almost every epidermal cell of the cotyledons, whereas wild-type seedlings accumulate AVIs in just a fraction of the cells. Similarly, vanadate-treated seedlings show a very significant increase of AVIs. Suggesting a role for autophagy in the formation of the AVIs, we show that various mutants (*atg* mutants) that interfere with the

autophagic process display reduced numbers of AVIs, often associated with significant alterations in the anthocyanin profiles. Our results suggest novel mechanisms for the formation of sub-vacuolar compartments capable of accumulating anthocyanin pigments.

RESULTS

Naringenin Addition Results in the Formation of New Anthocyanins

The addition of naringenin to *tt5* or wild-type seedlings grown in conditions that induce anthocyanin biosynthetic genes (AIC, Anthocyanin Inductive Conditions; Poustka et al., 2007) results in increased pigment formation compared to seedlings grown in identical conditions, but without naringenin. In addition, naringenin-treated seedlings accumulate significantly more AVIs than control ones, yet the number of AVIs does not directly correlate with total anthocyanin accumulation (Poustka et al., 2007). Naringenin has a modest effect on seedling germination or development at concentrations up to 100 μM (Supplemental Figure 1), the naringenin concentration used in all the experiments described in this study.

To determine whether the number of AVIs that accumulate in seedlings grown under AIC relate to a particular anthocyanin, rather than to total anthocyanin levels, we compared the HPLC anthocyanin profiles of wild-type and *tt5* seedlings grown in AIC, treated and not treated with naringenin. The *tt5* mutant is in the *Landsberg erecta* (*Ler*) genetic background, but, because we use Columbia (*Col*) in other sections of this study, we investigated here the anthocyanin profiles of both *Ler* and *Col* as wild-type lines. Thirteen anthocyanins were found in wild-type seedlings grown in AIC without naringenin, and we numbered the peaks here 1–13 (Figure 1 and Table 1). The anthocyanin profiles of *Ler* and *Col* seedlings are similar with regard to the types of anthocyanins that they accumulate (compare Figure 1A and 1C), but there are clear differences in the relative abundance of particular anthocyanins (e.g. peaks 6 and 7, Figure 1A and 1C). The addition of naringenin to *tt5* or to either of the two wild-types resulted in the appearance of at least four new anthocyanin peaks (a, b, c, and d in Figure 1), without a significant change in the relative abundance of the other anthocyanins (Figure 1). The flavonol profiles, however, remain similar between the wild-type lines, with and without naringenin. However, the *tt5* mutant, which normally has no flavonols, when complemented with naringenin, synthesized flavonols to levels approximately 30% of those present in *Ler* (not shown). These results are of significance because they suggest that despite the efficient uptake of naringenin by seedlings grown in AIC (Poustka et al., 2007), the levels of flavonoids in complemented *tt5* mutant fail to reach the levels in wild-type seedlings, perhaps suggesting an inefficiency of naringenin in reaching the biosynthetic complexes.

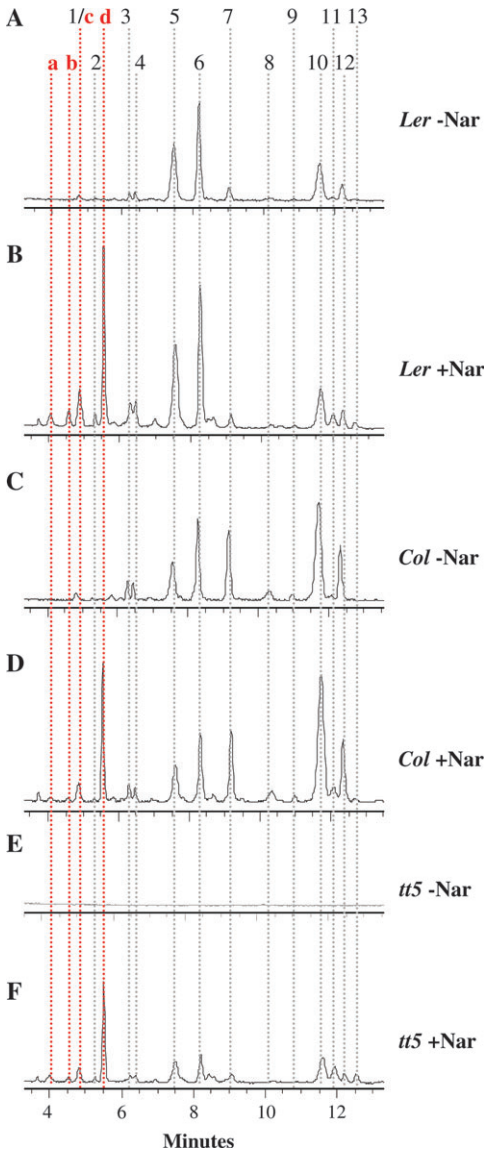

Figure 1. Anthocyanin Profiles of *Arabidopsis* Seedlings in the Presence or Absence of Naringenin.

HPLC chromatographic profiles of anthocyanins at 520 nm of 3-day-old wild-type (*Ler*) **(A, B)**; *Col* **(C, D)**; and *tt5* **(E, F)** grown in the absence (–Nar., A, C, and E) or presence (+Nar., B, D, and F) of 100 μM naringenin. Peaks 'a, b, c, and d' (red lines) correspond to anthocyanins newly accumulated upon the addition of naringenin. Peaks 1–13 correspond to anthocyanins previously described and characterized in Table 1. Anthocyanins were extracted from identical amounts of dry material, and the same volume was injected in each run.

To determine the identity of all the anthocyanins, we performed HPLC–MS/MS. Eight of the peaks match those as previously reported by Tohge et al. (2005) (Table 1). Several new anthocyanins were also detected in wild-type plants. Peak d, the most abundant one after the addition of naringenin, has a parent cation of 449.11 m/z and a fragment of 287.06 m/z, consistent with C3G (Table 1). Its identity as C3G was further confirmed by the UV-visible spectrum and its

Table 1. Characteristics of the Anthocyanin Peaks Identified in Figure 1.

Peak	Rt (min.)	λ features (nm)	ESI–MS (m/z)	MS/MS fragments (m/z)	MS[e] fragmentation (m/z)	*PAP1-D* (Tohge et al., 2005)
a	4.0	520	611.16	449 [Cy + Glc]$^+$ 287 [Cy]$^+$		
b	4.5	500	611.16	449 [Cy + Glc]$^+$ 287 [Cy]$^+$		
1	4.8	513	743.21	449 [Cy + Glc]$^+$ 287 [Cy]$^+$	581, 449, 287	
c		503	611.16	449 [Cy + Glc]$^{+1}$ 287 [Cy]$^+$		
2	5.2	530	949.27	449 [Cy + Glc]$^+$ 287 [Cy]$^+$	787, 449, 287	A4
d	5.5	516	449.11	287 [Cy]$^+$		
3	6.2	527	1137.32	889 [Cy + 2Glc + Xyl + Cou]$^+$ 535 [Cy + 2Glc + Mal]$^+$ 287 [Cy]+	975	A8
4	6.4	540	1343.47	1095 [Cy + 2Glc + Xyl + Cou + Sin]$^+$ 535 [Cy + 2Glc _ Mal]$^+$ 287 [Cy]$^+$	1095, 535	A11 (see Supp. Fig. 4)
5	7.5	520	1257.41	1095 [Cy + 2Glc + Xyl + Cou + Sin]$^+$ 449 [Cy + Glc]$^+$ 287 [Cy]$^+$	1137, 897, 889, 535, 287	A10
6	8.2	535	1343.54	1095 [Cy + 2Glc + Xyl + Cou + Sin]$^+$ 535 [Cy + 2Glc + Mal]$^+$ 287 [Cy]$^+$	1095, 535, 287	A11 (see Supp. Fig. 4)
7	9.0	530	1181.34	933 [C + Glc + Xyl + Sin + Cou]$^+$ 535 [Cy + 2Glc + Mal]$^+$ 287 [Cy]$^+$	975 727, 535, 287	A9
8	10.2	520	889.25	727 [Cy + Glc + Xyl + Cou]$^+$ 449 [Cy + Glc]$^+$ 287 [Cy]$^+$		A3
9	10.8	530	1095.31	933 [Cy + Glc + Xyl + Sin + Cou]$^+$ 449 [Cy + Glc]$^+$ 287 [Cy]$^+$		
10	11.6	525	975.24	727 [Cy + Glc + Xyl + Cou]$^+$ 535 [Cy + 2Glc + Mal]$^+$ 287 [Cy]$^+$		
11	11.9	326/ 535	1005.26	757 535 [Cy + 2Glc + Mal]$^+$ 287 [Cy]$^+$		
12	12.2	320/ 535	1181.33	933 [Cy + Glc + Xyl + Sin + Cou]$^+$ 535 [Cy + 2Glc + Mal]$^+$ 287 [Cy]$^+$		A9
13	12.6	326/530	1211.36		963, 535, 287	

Rt, retention time; Cy, cyanidin; Glc, glucose; Xyl, xylose; Cou, *p*-coumaroyl moiety; Mal, malonyl moiety; Sin, sinapoly moiety. The *PAP-1D* column corresponds to the anthocyanin names assigned in Tohge et al. (2005).

co-elution with an authentic C3G standard (Supplemental Figure 2). Peaks a, b, and c (each 611.16 m/z and co-eluting in extracts from wild-type plants) appear to correspond to cyanidin 3-*O*-diglucoside derivatives, based on the fragmentation profile (611 > 449 287 m/z). However, the structures of peaks a, b, and c have yet to be unequivocally established (Table 1).

We investigated the accumulation of the new peaks over time, after naringenin addition in *tt5*. C3G (peak d) appeared 3 h after naringenin addition, peaking at 12 h, to then decrease (Figure 2), while peaks a and b continued to increase, albeit at significantly lower levels than C3G. Peak c, although identified by LC–MS, co-eluted with peak 1 and could not be quantified by PDA–HPLC. Most other peaks remained unchanged (Supplemental Figure 3). Based on total absorbance at 520 nm (A_{520}), peaks a and b correspond respectively to ~1.8 and ~1.6% of the total anthocyanins present in *Ler* + Nar (24 h after Nar induction, Figure 1), while peak d corresponds to ~14.7%.

These results suggest that the addition of naringenin to *tt5* or wild-type *Arabidopsis* seedlings results in the accumulation of C3G, an anthocyanin normally absent in *Arabidopsis* under

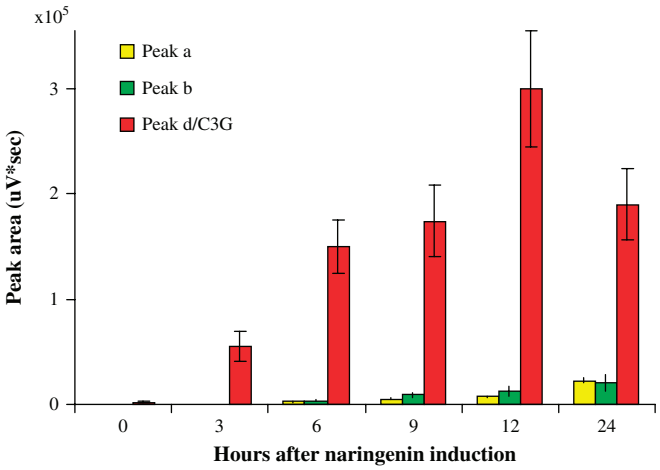

Figure 2. Time-Course Accumulation of Anthocyanin Peaks a, b, and c after Naringenin Addition.

Quantification of anthocyanin peaks a, b, and c in 3-day-old wild-type (*Ler*) seedlings treated with 100 μM naringenin for different (0, 3, 6, 9, 12, and 24-h) periods of time. The quantification is based on peak area (μVol*sec) measurements of HPLC chromatograms revealed at 520 nm.

normal growth conditions, yet likely a precursor in the accumulation of some of the more complex anthocyanins present (Supplemental Figure 4). In addition, several new anthocyanins with chemical structures yet to be determined were found to be present as well.

Increase in AVI Numbers in Anthocyanin 5-*O*-Glucosyltransferase (*5gt*) Mutants

Naringenin-supplemented seedlings accumulate significantly more AVIs than control plants (Poustka et al., 2007). To determine whether the accumulation of AVIs is directly linked to the increased accumulation of C3G or C3G derivatives, we investigated the AVI distribution of *5GT* mutant (*5gt*), which fail to conjugate a glycosyl group at the 5-*O* position of the anthocyanidin core (Tohge et al., 2005). In our induction conditions, the addition of naringenin increases the accumulation of anthocyanins in *5gt* to levels comparable to wild-type (Figure 3A, *5gt*), primarily as a consequence of the increase of C3G (compare peak d in Figure 3B and 3C).

To determine the identity of all the anthocyanins present in *5gt* grown in AIC, we performed HPLC–MS/MS. Ten new peaks have been identified and named 14–26 (Figure 3B and 3C and Table 2). Peaks a, b, c (611.16 m/z peaks), and d (449.11 m/z peak), previously identified in wild-type plants grown in AIC with naringenin, were also found in the *5gt* mutant and are the only ones in common by both m/z and elution time (Figure 3B–3D). Since *5gt* should be devoid of 5-*O*-glycosides, either the 611 species correspond to 3-*O*-glycosides or are glycosylated at a position other than 3-*O* or 5-*O*. Moreover, as both wild-type and *5gt* were induced with naringenin for these experiments, this could explain why 449 m/z was not previously detected (Tohge et al., 2005).

In wild-type, there is only one 743-m/z species, but in *5gt*, there are two 743-m/z peaks that do not co-elute with the species in wild-type, yet share the same accurate mass and anthocyanin PDA spectrum. Similar isobaric species were detected for 1181 m/z (two peaks) and 1343 m/z (two peaks) in wild-type extracts. In *5gt*, this trend towards isomers seems more prevalent with 743 m/z (two peaks), 889 m/z (four peaks), 727 m/z (two peaks), and 933 m/z (two peaks). Most of these multiples involve a dominant species, which are likely the single species previously identified (Tohge et al., 2005). The 889-m/z peaks in *5gt* (peaks 18–21, Figure 3B and 3C) are of particular interest, as there are four of them and of similar intensity. We expect they are positional isomers of the 889-m/z species in wild-type (peak 8, Figure 3D), as the 5-*O*-glucoside should not be available in *5gt*. Similarly, the 743-m/z species (peaks 14 and 15, Figure 3B and 3C) and the 1095-m/z specie (peak 22, Figure 3B and 3C) in *5gt* are likely an isomer of the 743-m/z (peak 1, Figure 3D) and 1095-m/z (peak 9) species in wild-type, respectively (Figure 3D and Table 1). Perhaps, in the absence of 5GT activity, 3GT or another glycosyl transferase can introduce elsewhere similar modifications to those present in the 5-*O* position of groups 1–3. Establishing this will require the structural elucidation of these compounds by NMR. Our

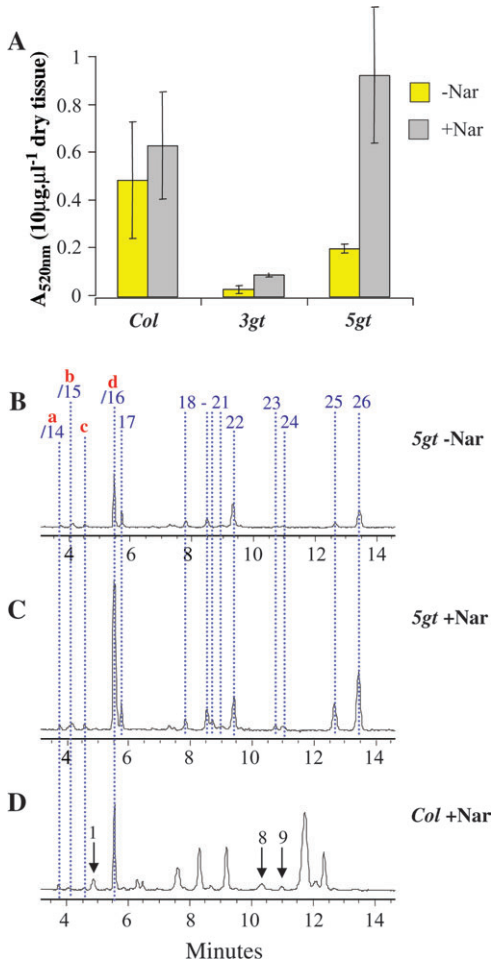

Figure 3. Anthocyanin Accumulation in *3gt* and *5gt* Seedlings.

(A) Spectrophotometric measurement (520 nm) of anthocyanin contents of *3gt*, *5gt*, and wild-type (*Col*) seedlings grown in AIC in the absence (–Nar) or presence (+Nar) of 100 µM naringenin. Anthocyanin accumulation levels correspond to arbitrary units obtained by dividing the absorbance at 520 nm by the mass of the starting plant material and the volume fraction used in the measurements.

(B–D) Chromatographic profiles (520 nm) of *5gt* and *Col* 3-day-old seedlings grown in the absence (A) or presence (B and C) of 100 µM naringenin.

studies highlight the value of exploring the metabolic space of mutants as a way to uncover novel catalytic functions obscured in wild-type plants.

In contrast to *5gt*, *3gt* mutant accumulate almost no anthocyanins, and the addition of naringenin resulted in a very modest increase (Figure 3A, *3gt*), providing evidence that 3-*O* glycosylation is necessary prior to 5-*O* glycosylation.

When *5gt* seedlings were visualized under the microscope, a very significant induction of AVIs became evident. Almost every single cell in the adaxial epidermal layer of the cotyledon displayed at least one AVI (compare Figure 4A and 4C, Figure 4G and 4H), regardless of whether the media were supplemented with naringenin or not (Figure 5A). As expected, no AVIs were observed in the *3gt* mutant (Figures 4E and 5A).

Table 2. Characteristics of the Anthocyanin Peaks Identified in the *5gt* Mutant + Naringenin.

Peak	Rt (min.)	λ features (nm)	ESI–MS (m/z)	MS[e] fragmentation (m/z)
14	4.0	510	611.16	287
a		511	743.21	287
15	4.5	511	611.16	287
b		504	743.21	287
c	4.8	505	611.16	287
16	5.5	516	581.15	287
d		515	449.11	287
17	5.7	532/332	787.21	
18	7.7	527	889.25	449
19	8.4	522	889.25	727
20	8.6	519	889.25	727, 449
21	8.9	510	889.25	727, 449
22	9.2	537/318	1095.32	
23	10.6	538/287	933.25	287
24	10.9	527/320	727.19	287
25	12.6	523/311	727.19	287
26	13.4	535/320	933.25	287

Rt, retention time.

These results indicate that the *5gt* mutation dramatically increases the formation of AVIs. The increased accumulation of AVIs in the *5gt* mutant is not restricted to seedlings grown in AICs. When we examined 3-week-old seedlings grown in plates under standard growth conditions, large numbers of AVIs were found in a region of the stem (Supplemental Figure 5). A similar accumulation of AVIs in *5gt*, but not in the wild-type, was observed in rosette leaves (Supplemental Figure 5). These results suggest that the increased formation of AVIs is a general characteristic of anthocyanin accumulating cells in the *5gt* mutant.

Previously, we showed that vanadate was a strong inducer of AVI formation in wild-type or naringenin-complemented *tt5* seedlings (Poustka et al., 2007). The addition of vanadate did not induce AVI formation in the *3gt* mutant (Figures 4F and 5A). In *5gt* seedlings, AVIs in every cell continued to form, irrespective of whether vanadate was present or not (Figures 4D and 5A), the bluish color reflecting the alkalinization of the vacuole induced by vanadate (Poustka et al., 2007).

AVIs Are Likely Formed by the Filling of Pre-Existing Sub-Vacuolar Structures

We described before that neutral red (NR) stains *Arabidopsis* sub-vacuolar structures (referred to hereafter as NRSB for NR-staining bodies) (Poustka et al., 2007). NR also stains the AVIs, and the number of cells with NRSB is always significantly larger than the number of cells with AVIs (compare *Col* in Figure 5A and 5B) (Poustka et al., 2007), suggesting that the detection of the NRSBs with NR is more sensitive than the coloration of the AVI provided by the anthocyanins, or that sub-vacuolar inclusions without anthocyanins exist.

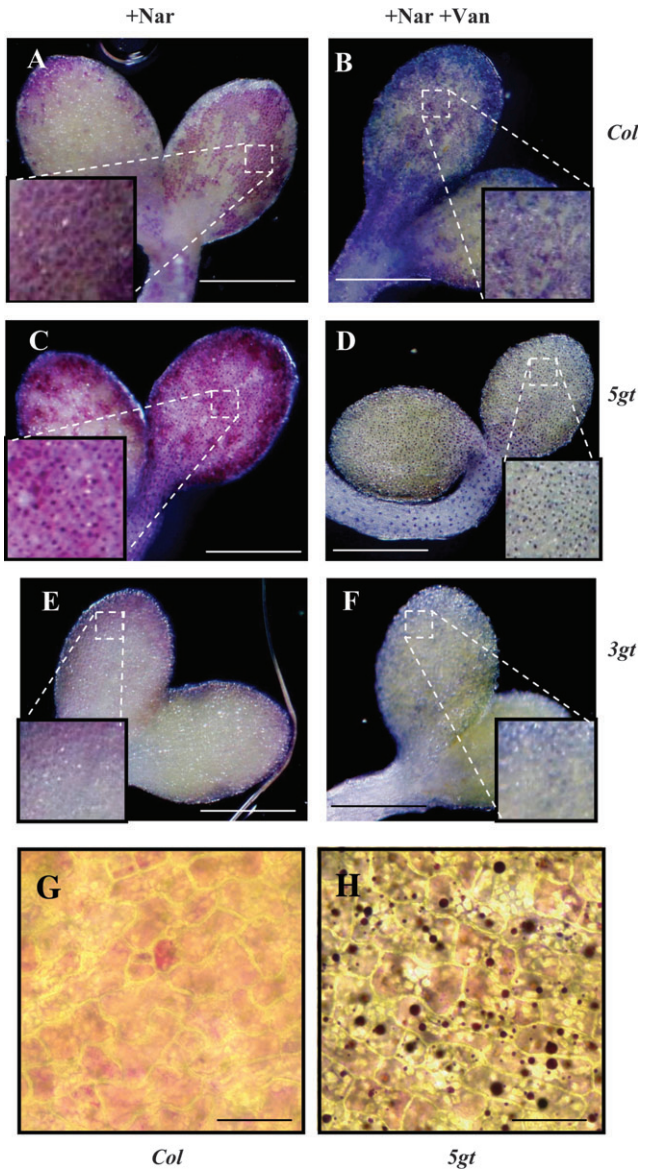

Figure 4. AVI Formation in *3gt* and *5gt* Seedlings.
(A–F) Three-day-old *3gt* and *5gt* mutants and wild-type (*Col*) seedlings treated with 100 μM naringenin (+Nar), treated or not treated with 1 mM vanadate (Na_3VO_4, +/–Van). Scale bars: A–F: 0.5 mm.
(G, H) Microscopic view of *Col* and *5gt* mutant cells (adaxial side of the cotyledons), treated with 100 μM naringenin (+Nar). Scale bar G–H: 30 μm.

To investigate the contribution of the different anthocyanins in AVI formation, we examined NRSBs in the *3gt* and *5gt* mutants. About 10–25% of the abaxial epidermal cells of the cotyledons of *Col* seedlings grown in AIC contain NR-staining sub-vacuolar structures (Figure 5B). This number does not significantly change in the presence of naringenin (compare –Nar and +Nar, Figure 5B). The *3gt* mutant accumulates significantly less NRSB than *Col*, with a slight induction in

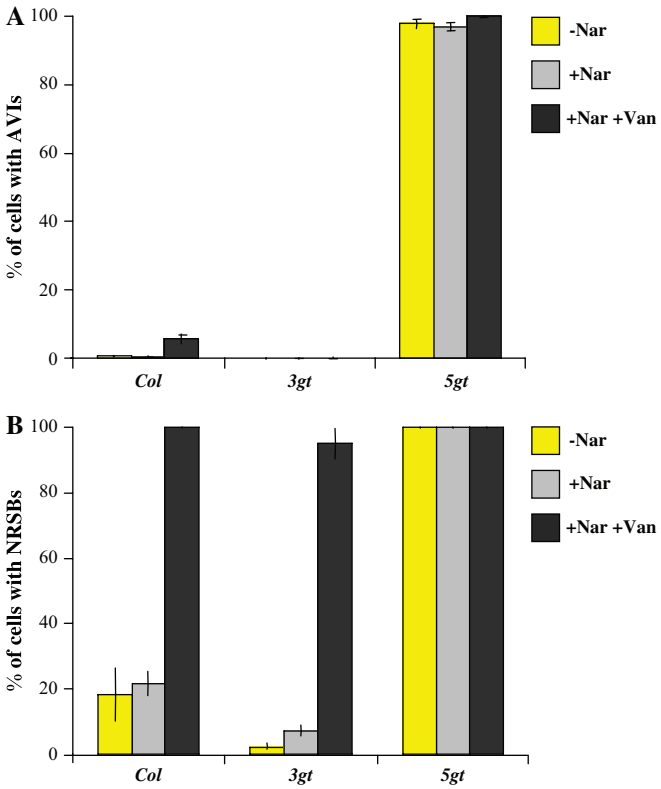

Figure 5. Quantification of AVI and NRSB Numbers in *3gt*, *5gt*, and *Col* Seedlings Induced with Naringenin.

(A) Number of AVIs and **(B)** number of neutral red staining sub-vacuolar structures (NRSBs) present in *5gt* and wild-type (*Col*) seedlings treated with 100 μM naringenin (+Nar), treated or left untreated with 1 mM vanadate (+/–Van). Seedlings were observed 24 h after the addition of naringenin and vanadate.

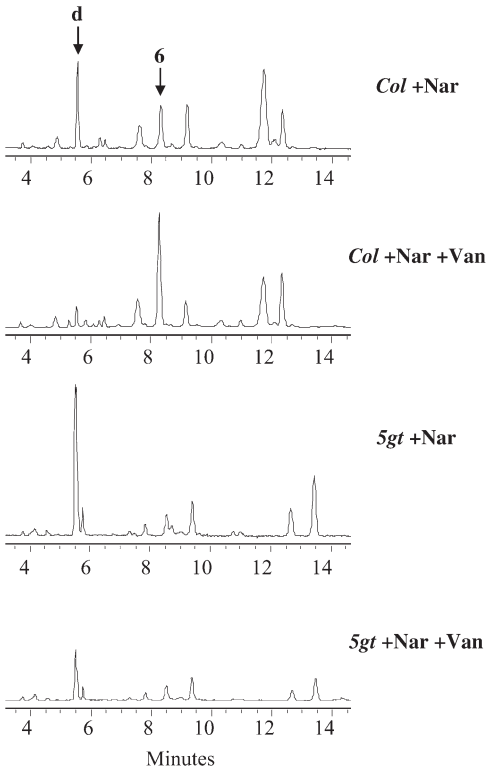

Figure 6. Effect of Vanadate on Anthocyanin Profiles.

HPLC chromatograms of anthocyanins (520 nm) of 3-day-old wild-type (*Col*) or *5gt* seedlings grown in the presence (+Nar) of 100 μM naringenin, with or without the addition of 1 mM vanadate (+/–Van).

the NRSB numbers when the seedlings were grown in the presence of naringenin (Figure 5B). This is in sharp contrast to the *5gt* mutant, in which every single cell shows NRSB (Figure 5B) filled with anthocyanins (Figures 4C and 5A). Interestingly, vanadate induces the formation of NRSB in *Col* and in *3gt* to levels similar to those found normally in the *5gt* mutant (Figure 5B). A similar ability of vanadate to induce NRSB in almost every cell was observed in *tt5* seedlings and in other pathway mutants, including *tt3* (mutant in dihydroflavonol reductase, DFR) and *tt19* (a mutant in a GST) (not shown). These results demonstrate that the formation of NR-staining sub-vacuolar compartments is independent of anthocyanin accumulation. Moreover, these results suggest that anthocyanins accumulating in the vacuolar sap might be taken up by these NRSBs, resulting in AVIs. Alternatively, a particular type of anthocyanin-filled NRSBs (visualized as AVIs) could form *de novo*, perhaps as part of the vacuolar uptake of anthocyanin-containing cytoplasmic vesicles (Poustka et al., 2007).

We next evaluated the possibility that particular anthocyanin(s) would be associated with AVI formation, by examining the effect of vanadate on the distribution of the various anthocyanins. Interestingly, while naringenin induced C3G (peak d, Figure 6), vanadate reduced C3G accumulation and instead resulted in the induction of peak 6 (Figure 6, compare *Col* + Nar and *Col* + Nar + Van). According to the MS analysis, peak 6 corresponds to A11 (Tohge et al., 2005), the most highly decorated anthocyanin found in *Arabidopsis* (Supplemental Figure 4). Consistent with peak 6 being modified at both the 3-*O* and 5-*O* positions, in the *5gt* mutant, vanadate causes an overall decrease in anthocyanin accumulation without any peak increasing (Figure 6, compare *5gt* + Nar and *5gt* + Nar + Van). We conclude from these results that while the presence of C3G (or derivatives) can be associated with AVI formation, as is the case in the *5gt* mutant, the mechanism by which vanadate induces AVIs involves the increased accumulation of compounds also modified at the 5-*O* position.

These results provide strong evidence that the NRSBs correspond to sub-vacuolar structures that exist even in the absence of anthocyanins. The formation of NRSBs dramatically induced by vanadate, and when anthocyanins accumulate, the NRSBs serve as an accumulation site for them, resulting in the AVIs. Some anthocyanins, in particular C3G and derivatives, appear to preferentially accumulate inside NRSBs, explaining the observation that all NRSBs are AVIs in *5gt* mutants. However, these results also suggest that the *5gt* mutant has the ability to form more NRSBs than wild-type, prompting the question of how the NRSBs form.

Autophagy and AVI Formation

To determine whether an autophagic mechanism participates in AVI formation, we investigated the effect of mutations in genes that participate in autophagy on AVI and NRSB formation. We had previously examined the effect of the *atg7-1* mutant on AVI formation, and we could not observe a significant difference in the number of NRSBs or AVIs when *atg7-1* seedlings were grown under AIC, compared to a wild-type ecotype Ws (Wassileskija) control. Ws seedlings accumulate a low level of anthocyanins and have significantly reduced numbers of AVIs and NRSBs compared to *Col* or *Ler* (Poustka et al., 2007).

Thus, we obtained *atg5*, *atg9*, and *atg10* mutants in the *Col* background. ATG5 is an autophagic protein that forms a conjugate with the ubiquitin-like protein, ATG12. This conjugation is essential for the formation of sequestering vesicles, and hence for plant nutrient recycling. The *atg5* mutant displays early senescence and *atg5* plants are hypersensitive to nitrogen or carbon starvation, accompanied by a more rapid loss of organellar and cytoplasmic proteins (Thompson et al., 2005). The ATG12–ATG5 conjugation is directed by ATG7, an E1-like ATP-dependent activating enzyme (Doelling et al., 2002), and the E2-like protein, ATG10. The *atg10* mutant is hypersensitive to nitrogen and carbon starvation and initiates senescence and programmed cell death more quickly than wild-type (Phillips et al., 2008). ATG9 is an integral membrane protein that may be required for membrane delivery for the growing of pre-autophagosomal structures (Nair and Klionsky, 2005).

While all the *atg* mutants tested appear to have normal anthocyanin levels at 4 d after germination (DAG), a significant reduction was observed for *atg5* ($P = 0.002$, two-sided *t*-test) and *atg10* ($P = 0.054$, two-sided *t*-test) at 5 DAG (Figure 7A and 7B). The anthocyanin profiles in the *atg* mutants also show distinctive patterns, particular at 5 DAG (Figure 8). Most anthocyanin peaks are significantly reduced in *atg5*, but peak 6 appears to be the most significantly affected, particularly when considered in relation to some of the other major anthocyanins present. The addition of vanadate to *atg5* further reduces peak 6. A similar situation is observed for *atg10*, although, in this case, vanadate has no additional effect on peak 6. In contrast, no major effect on anthocyanin profiles was observed for *atg9*, even after the treatment with vanadate (Figure 8). These results indicate that, despite all the *ATG* genes being part of a common cellular process, each mutant has a unique fingerprint when it comes to anthocyanin accumulation. In addition, each *atg* mutant responds in a unique way to the treatment of vanadate, with respect to anthocyanin profiles.

We next investigated the number of AVIs present at 4 and 5 DAG. The *atg5* and *atg10* mutants displayed a very significant reduction in the overall numbers of AVIs. No AVIs could be observed in *atg5* seedlings at either age, and *atg10* had no detectable AVIs at 5 DAG (Figure 9A). When we stained with NR, *atg5* and *atg10* showed a significantly lower number of

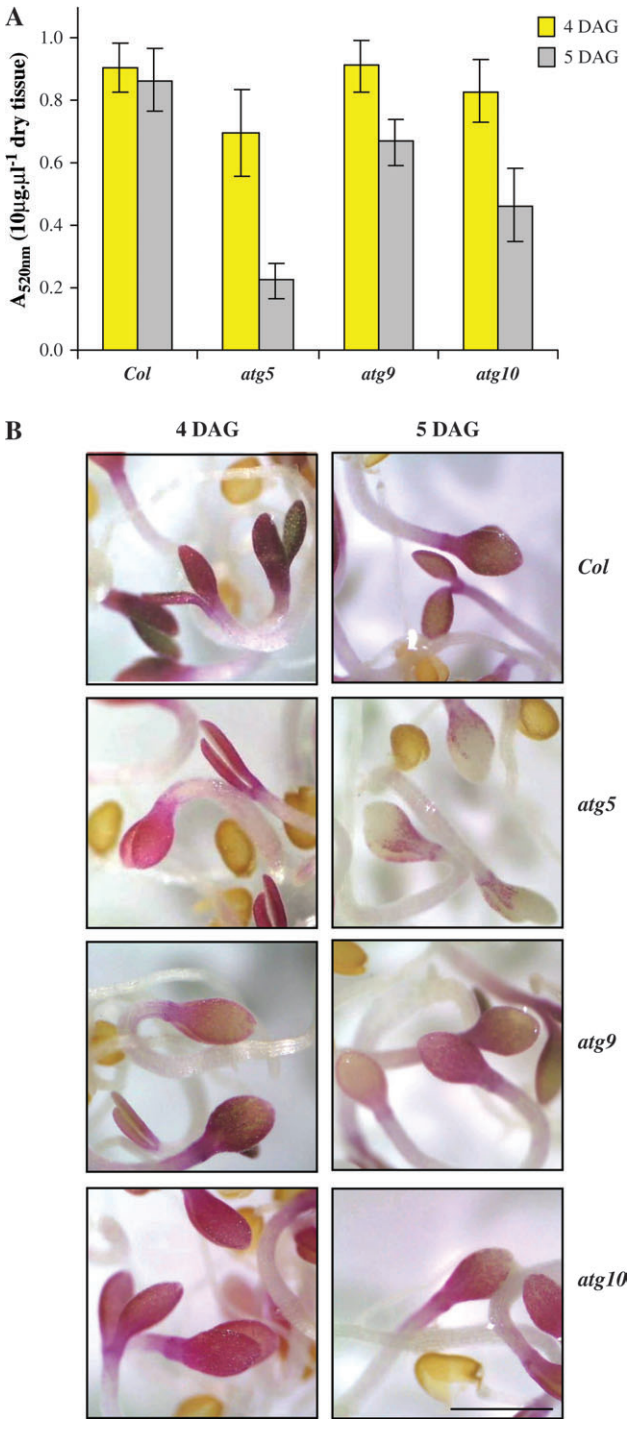

Figure 7. Autophagic Mutants and Anthocyanin Accumulation.

(A) Spectrophotometric measurement (520 nm) of anthocyanin content of *atg5*, *atg9*, *atg10*, and wild-type (*Col*) seedlings 4 and 5 d after germination (DAG) grown in AIC. Anthocyanin accumulation levels correspond to arbitrary units obtained by dividing the absorbance at 520 nm by the mass of the starting plant material and the volume fraction used in the measurements.

(B) Microscopic pictures of *atg5*, *atg9*, *atg10*, and wild-type (*Col*) seedlings 4 and 5 days after germination (DAG) grown in AIC.

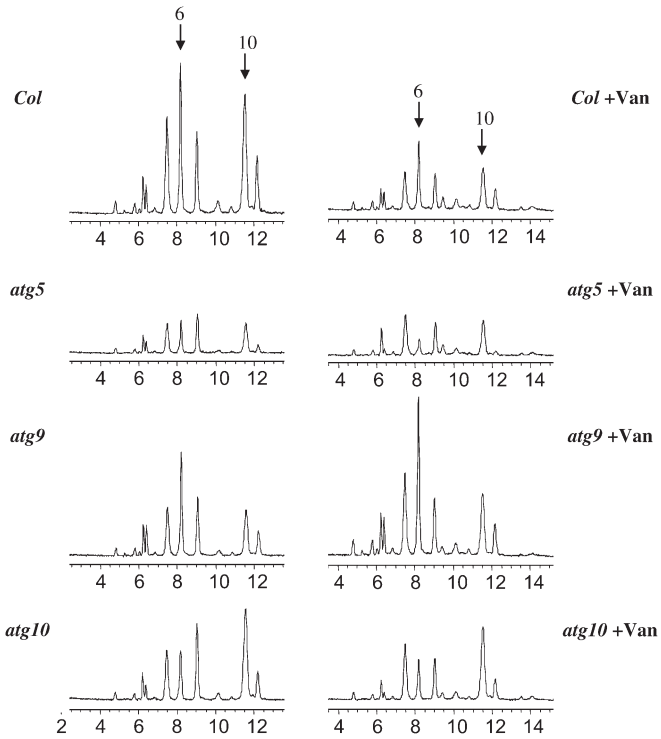

Figure 8. Autophagic Mutants and Anthocyanin Profiles.

HPLC chromatograms of anthocyanins (520 nm) of *atg5*, *atg9*, *atg10*, and wild-type (*Col*) seedlings 5 DAG grown in AIC in the absence (left panel) or presence of 1 mM vanadate (Van).

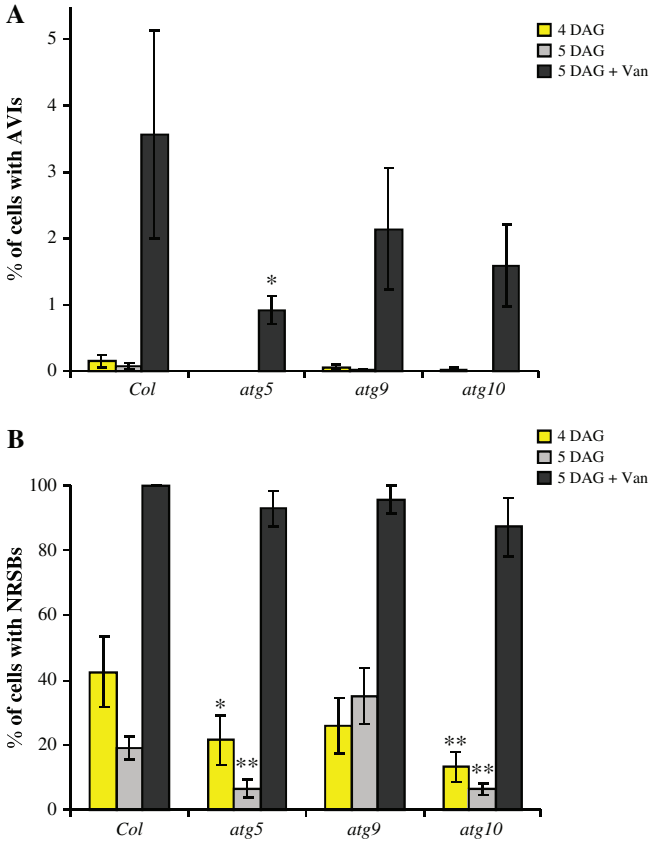

Figure 9. AVI and NRSB Formation in Autophagic Mutants.

(A) Number of AVIs and **(B)** number of neutral red staining sub-vacuolar structures (NRSBs) present in *agt* mutants and wild-type (*Col*) seedlings 4 or 5 DAG treated with 100 μM naringenin (+Nar), treated or left untreated with 1 mM vanadate (Van). Seedlings were observed 24 h after the addition of naringenin and/or vanadate. Asterisks indicate a significant difference compared to the wild-type values (one asterisk: $P < 0.1$; two-sided *t*-test and two asterisks: $P < 0.05$; two-sided *t*-test).

NRSB compared to wild-type, while the levels in *atg9* appear to be lower at 4 DAG but increase above the *Col* control at 5 DAG (Figure 9B). It is apparent that there is an overall reduction in AVIs and NRSBs as the seedlings become older (compare *Col* 4 and 5 DAG, Figure 9A). The treatment with vanadate, however, resulted in the increased formation of AVIs (Figure 9A) and NRSBs (Figure 9B). Interestingly, while vanadate induces NRSB formation in 100% of the epidermal cells in wild-type plants, the number of NRSBs in vanadate-treated *atg* mutants never reaches wild-type levels (Figure 9B). Time-course experiments following the number of NRSBs in wild-type and *atg5* after vanadate treatment further showed a very slow increase in the number of NRSBs compared with a very rapid increase in wild-type (not shown). Taken together, these results suggest a significant participation of an autophagic mechanism in the formation of the NRSBs, which is further accentuated in the capacity of these structures to become AVIs.

DISCUSSION

In this study, we investigated the relationship between the accumulation of particular anthocyanins, the formation of AVIs and vacuolar transport mechanisms to gain a better understanding of the relationship between transport and sequestration of these pigments. We established that the addition of naringenin to *tt5* or wild-type seedlings results in increased C3G accumulation and AVI formation. We determined that the *5gt* mutant, which is unable to glycosylate C3G and derivatives at the 5-*O* position, increases dramatically AVI numbers. Finally, by investigating several autophagic mutants, we concluded that autophagy participates in the formation of NRSBs and AVIs. We propose the following models to explain our results.

We hypothesize that autophagy participates in the formation of the NRSB and that these structures could correspond to autophagic bodies. This is consistent with the low numbers normally present in wild-type *Arabidopsis*, since, as soon as autophagic bodies form, they are broken down by vacuolar resident hydrolases (Thompson and Vierstra, 2005). When anthocyanins accumulate, as is the case for wild-type seedlings grown under AICs, anthocyanins accumulate in NRSBs, which are visualized as AVIs. The percentage of cells with AVIs remains low (<10% of cotyledon epidermis), because these

structures continue to be subjected to the normal autophagic body breakdown, releasing anthocyanins to the vacuolar sap. The treatment with vanadate, which results in a significant alkalanization of the vacuole (Poustka et al., 2007), may inhibit the normal dissolution of the autophagic bodies (as is the case for concanamycin A, an attenuator of autophagic bodies breakdown; Thompson and Vierstra, 2005). Vanadate is not typically utilized as an inhibitor of autophagy, yet it has been shown to inhibit autophagy in animals (Fosse et al., 1995) and yeast (Kim and Klionsky, 2000), although it is more likely involved in the cytoplasmic formation of the autophagosome, rather than in autophagic body breakdown. However, it is possible that, as is the case for the yeast aminopeptidase I (API) resident vacuolar enzyme, a cytoplasm-to-vacuole autophagic mechanism is involved in the import of hydrolytic enzymes that participate in authophagic body breakdown (Kim and Klionsky, 2000). Indeed, the disruption of vacuolar trafficking mechanisms leads to autophagy-related phenotypes, likely through defects in the delivery of hydrolases to the vacuole (Zouhar et al., 2009). Therefore, directly or indirectly, vanadate could inhibit autophagic body breakdown, resulting in the accumulation of NRSBs, irrespective of whether anthocyanins are present or not (as shown for the *3gt* mutant, Figure 5B). However, when anthocyanins are present, then they preferentially accumulate inside these structures, resulting in the high AVI numbers observed (Figure 5A). Our results are, however, also consistent with the possibility that a particular flavonoid/anthocyanin induces autophagy. Flavonoids play multiple signaling functions in cells (Peer and Murphy, 2006; Pourcel and Grotewold, 2009; Taylor and Grotewold, 2005), and perhaps the excess accumulation of particular flavonoids triggers an auophagic process by which ER-derived compartments filled with flavonoids (Poustka et al., 2007) are taken up by the vacuole.

The relationship between AVIs and C3Gs (including C3G derivatives) can be explained by two non-exclusive models. According to the first model, perhaps C3Gs, but not the normal anthocyanins present in *Arabidopsis* (which all have 5-*O* glycosylation, Supplemental Figure 4), naturally inhibit autophagosome breakdown. Since the addition of naringenin results in increased C3G formation (Figure 1), this causes AVIs to form at levels that cannot be simply explained by the total anthocyanin levels (Poustka et al., 2007). Similarly, the *5gt* mutant that accumulates only C3Gs builds up AVIs in all cells (Figures 4 and 5). This model could explain the variable presence of AVIs in different plants—perhaps only those plants accumulating particular C3G derivatives would contain AVIs. A corollary of this model is that the AVIs may have a specific affinity for C3Gs. However, the treatment with vanadate, which results in a significant increase in AVIs (Figure 5A), shows decreased C3G accumulation, and only peak 6 increases in these conditions (Figure 6), suggesting that C3G alone is not sufficient for the formation of the AVIs. Flux analyses will be required to investigate whether the vanadate-dependent reduction in C3G accumulation reflects reduced C3G synthesis/transport to the vacuole, or increased C3G degradation.

Alternatively, C3G and C3,5G derivatives might be transported to the vacuole by different mechanisms. Indeed, they might have different fates immediately after biosynthesis, perhaps even be synthesized by different metabolons on the cytoplasmic surface of the ER. C3,5Gs might correspond to the compounds that accumulate in the lumen of the ER and are transported through vesicles to the vacuole (Poustka et al., 2007). An autophagic mechanism, similar to that involved in the delivery of storage proteins or rubber particles from the ER to the vacuole (CVT-like process in Thompson and Vierstra, 2005), would then be responsible for the formation of autophagic bodies, which could coalesce and result in the AVIs. Indeed, we have observed small anthocyanin-containing structures in the lumen of *Arabidopsis* vacuoles (not shown). Environmental conditions, such as light, might control the fusion of these small structures into large AVIs, in a process similar to that which we described for maize (Irani and Grotewold, 2005). In contrast, C3Gs might be taken up by the vacuole by a vanadate-sensitive transport mechanism, explaining why vanadate specifically affects peak d (Figure 6). Once in the vacuole, particular C3G and C3,5G derivatives would be sequestered inside AVIs.

Taken together, these results provide evidence for the existence of sub-vacuolar compartments in *Arabidopsis* that can be filled with anthocyanins under specific conditions, such as the increased accumulation of particular anthocyanins. Our results provide links between the formation of these structures and autophagic mechanisms, suggesting interesting relationships between anthocyanin sequestration and cellular metabolic status. Furthermore, from an applied perspective, AVIs are an attractive feature to achieve when engineering flower color. AVIs often result in a deeper hue, as seen in maize and rose (cv. Rhapsody in Blue) (Gonnet, 2003; Irani and Grotewold, 2005). Effectively knocking out *5GT* function in floricultural-important species may result in new varieties with altered flower color.

MATERIALS AND METHODS

Plant Materials and Growth Conditions

The *Arabidopsis* (*Arabidopsis thaliana*) *CHI* mutant (*tt5-1*), 3-*O*-glucosyl transferase At5g17050 (*3gt*, Salk_049338), 5-glucosyltransferase At4g14090 (*5gt*, Salk_108458), were obtained from the Arabidopsis Biological Resource Center (ABRC, Columbus, OH). The autophagic mutants *atg5* (At5g17290, N823856), *atg9* (At2g31260, N645980), and *atg10* (At3g07525, N645980) were obtained from Heike Lenz and Thorsten Nuernberger (University of Tübingen, Germany) and Richard Vierstra (University of Wisconsin, WI). For experiments involving the induction of anthocyanins in seedlings (AIC, anthocyanin inductive conditions), seeds were surface-sterilized and plated in water containing 3% sucrose. After 3 d of stratification at 4°C, seeds were germinated for 3 d at 25 $\pm$ 2°C in continuous cool-white light (GE F30T12-CW-RS) at approximately 100 $\pm$ 10 μmol m^{-2} s^{-1} on a rotary shaker.

Treatment of *Arabidopsis* Seedlings with Various Chemicals

For the naringenin treatments, seedlings were allowed to grow for 3 d and then naringenin (Sigma-Aldrich) was added to a final concentration of 100 μM from a 100-mM stock (in ethanol). For vanadate treatments, 3-day-old seedlings were preincubated with 1 mM vanadate (Sigma, stock solution 1 M sodium orthovanadate in water) for 1 h at 25 ± 2°C before the addition of naringenin. Each treatment was done at least in triplicate. Naringenin inhibition studies were carried out in MS medium (Murashige and Skoog, 1962) with 3% sucrose, solidified with 0.7% agar. Seeds were plated on MS plates, cold-treated for 2 d at 4°C, and grown vertically in the growth chamber. Four to 5-day-old seedlings, whose roots were ~1.5 cm long, were transferred aseptically to new MS plates with naringenin concentrations ranging from 0 to 500 μM. The seedlings were aligned in a straight line, 1 cm apart. Growth was observed at an end point of 10 d after transfer.

Anthocyanin Extraction, Analysis, and Quantification

After the various treatments, seedlings were harvested, rinsed with water, and lyophilized for 2 d. Dry weight was measured and soaked overnight at room temperature in 50% methanol in water or 50% (v/v) methanol (MeOH)–3% (v/v) formic acid (FA) in water to get a final suspension of 50 mg mL^{-1} (w/v). Two volumes of 1% (v/v) HCl in 50% MeOH or 3% (v/v) FA in water were added to the methanolic extracts, and absorption was evaluated at 520 nm, using a Cary 50 UV-VIS spectrophotometer (Varian) in 40 μL quartz microcuvettes. The HPLC analysis of flavonoids and anthocyanins was carried out by adding one volume of 3% (v/v) FA in water to the methanolic extract, and separating 10 μL of the extract on a C18 column (Symmetry 4.6 × 75 mm, 3.5 μm) using a Waters Alliance 2695 separations module equipped with a 2996 photodiode array detector and a fluorescence detector (Waters Corporation). Flavonoids were separated using solvent A: 5% (v/v) FA in water; solvent B: 5% (v/v) FA in acetonitrile. Chromatograms and spectra were extracted and analyzed with Empower software (Waters Corporation). HPLC–mass spectrometric analyses were performed as described in the following section.

HPLC–MS/MS Analysis of Anthocyanins in *Arabidopsis* Extracts

In addition to HPLC–PDA analysis of anthocyanins, HPLC–MS/MS was carried out on extracts to identify the PDA peaks. To this end, 50–100 μL of extract were introduced to a 2695 Alliance HPLC system (Waters Corp., Beverley, MA) including two Symmetry C18 columns (each 4.6 × 75 mm, 3.5 μm; Waters Corp.) connected in series. A solvent system of 5% (v/v) formic acid in water as (A) and 5% (v/v) formic acid in acetonitrile as (B) was used to separate the compounds starting with 100% A with a linear gradient to 25% B over 20 min, ramp to 80% B over 2 and 3 min to re-equilibrate to initial conditions. The column temperature was 35°C and the flow rate was 1.0 mL min^{-1}. Eluent from the HPLC column first passed through a photodiode array (PDA) detector (Model 996, Waters Corp.) collecting absorbance spectra from 200 to 700 nm. From the PDA, the eluent was split to send approximately one-tenth of the flow to an electrospray (ESI) probe, which interfaced with a quadrupole-time-of-flight mass spectrometer (QTof Premier, Micromass, Manchester, UK) operated in positive ion mode. Probe and source conditions included capillary voltage of 3.2 kV, 400°C desolvation temperature, 50 L h^{-1} cone gas, 400 L h^{-1} desolvation gas, 110°C block temperature.

Two experimental MS approaches were brought to task on these samples: (1) MS^e Tof MS and (2) QTof MS/MS, both in conjunction with PDA information (520-nm absorbance peaks) in order to identify anthocyanin peaks. In MS^e, the instrument cycles between two types of acquisition, a low-energy and a high-energy scan, from 50 to 1500 m/z. In the low-energy scan, the collision energy is set to 8 eV to permit parent ions to reach the detector without fragmenting. In the high-energy scan, collision energy is ramped from 20 to 30 eV to indiscriminately fragment whatever ions are in the collision cell (collisionally induced dissociation, CID) at the time. This allows one to quickly survey for parent/daughter ion relationships (inferred by coincident PDA 520 nm) without knowing the species in advance. It also yields some fragment information that generally agrees with true MS/MS functions where the quadrupole selects a particular parent, sending only it to the CID for fragmentation. For the most abundant anthocyanins detected in the first mode, a run involving true MS/MS was performed to confirm the aglycone and surmise glycosylating sugars according to neutral loss. Thus, in the high-collision energy scan, we observed 287-m/z cations, representing cyanidin fragmented from the parent molecules. Kaempferol also has an m/z of 287 and could be confused with cyanidin, although its lambda max is 350 nm. When a 287-m/z fragment was detected that had a coincident 520-nm peak without significant 350-nm peak, it was presumed to be a kaempferol glycoside. Acylated cyanidin glycosides present a notable 320-nm shoulder used to identify acylations with phenolic acids. The ToF analyzer yields m/z of ions with an accuracy of <2 ppm. By combining the accurate mass of the ions and fragments with co-migration to A_{520}-nm peaks (PDA), a good deal of confidence can be gained in these identifications. Our tentative identifications based on MS results were compared to the results of Tohge et al. (2005) and, together, contribute to the patterns of glycosylation and acylation reported.

Microscopy

Neutral red (NR, Sigma) was dissolved in water and used at a final concentration of 1 mg mL^{-1}. Seedlings were incubated with NR for 20 min at room temperature. For quantifying AVIs, abaxial epidermal cells of cotyledons containing at least one AVI were counted and compared to the total number of cells

of the abaxial surface. Total cells were calculated by multiplying the number of vertical cells by the number of horizontal cells of the entire adaxial surface. Samples were examined using bright light of a Nikon Eclipse 600 microscope (Nikon) and Olympus stereomicroscope.

SUPLEMENTARY DATA

Supplementary Data are available at *Molecular Plant Online*.

FUNDING

This work was supported by the National Science Foundation (grant no. MCB–0130062 to E.G.).

ACKNOWLEDGMENTS

We are thankful to Kazuky Saito, Richard Vierstra, Heike Lenz, and Thorsten Nuernberger for sharing with us several mutants and unpublished information, and Gregory Hostetler for technical help. We appreciate the financial support for the Plant Biotech Center Metabolomics Facility provided by the OSU Plant-Microbe Genomics Facility. No conflict of interest declared.

REFERENCES

Bassham, D.C. (2007). Plant autophagy: more than a starvation response. Curr. Opin. Plant Biol. **10,** 587–593.

Buchanan, B., Gruissem, W., and Jones, R. (2000). Biochemistry and Molecular Biology of Plants (Rockville: ASPP).

Conn, S., Zhang, W., and Franco, C. (2003). Anthocyanic vacuolar inclusions (AVIs) selectively bind acylated anthocyanins in *Vita vinifera* L. (grapevine) suspension culture. Biotech. Ltrs. **25,** 835–839.

Debeaujon, I., Peeters, A.J.M., Leon-Kloosterziel, K.M., and Koornneef, M. (2001). The *TRANSPARENT TESTA12* gene of *Arabidopsis* encodes a multidrug secondary transporter-like protein required for flavonoid sequestration in vacuoles of the seed coat endothelium. Plant Cell. **13,** 853–871.

Doelling, J.H., Walker, J.M., Friedman, E.M., Thompson, A.R., and Vierstra, R.D. (2002). The APG8/12-activating enzyme APG7 is required for proper nutrient recycling and senescence in *Arabidopsis thaliana*. J. Biol. Chem. **277,** 33105–33114.

Fosse, M., Berg, T.O., O'Reilly, D.S., and Seglen, P.O. (1995). Vanadate inhibition of hepatocytic autophagy: calcium-modulated and osmolality-modulated antagonism by asparagine. Eur. J. Biochem. **230,** 17–24.

Gonnet, J.F. (2003). Origin of the color of Cv. Rhapsody in Blue rose and some other so-called 'blue' roses. J. Agric. Food Chem. **51,** 4990–4994.

Goodman, C.D., Casati, P., and Walbot, V. (2004). A multidrug resistance–associated protein involved in anthocyanin transport in *Zea mays*. Plant Cell. **16,** 1812–1826.

Gould, K.S. (2004). Nature's swiss army knife: the diverse protective roles of anthocyanins in leaves. J. Biomed. Biotechnol. **2004,** 314–320.

Grotewold, E. (2006). The genetics and biochemistry of floral pigments. Annu. Rev. Plant Biol. **57,** 761–780.

Grotewold, E., and Davis, K. (2008). Trafficking and sequestration of anthocyanins. Nat. Prod. Comm. **3,** 1251–1258.

Grotewold, E., et al. (1998). Engineering secondary metabolism in maize cells by ectopic expression of transcription factors. Plant Cell. **10,** 721–740.

Hsieh, K., and Huang, A.H. (2007). Tapetosomes in *Brassica tapetum* accumulate endoplasmic reticulum-derived flavonoids and alkanes for delivery to the pollen surface. Plant Cell. **19,** 582–596.

Irani, N.G., and Grotewold, E. (2005). Light-induced morphological alteration in anthocyanin-accumulating vacuoles of maize cells. BMC Plant Biology. **5,** 7.

Kim, J., and Klionsky, D.J. (2000). Autophagy, cytoplasm-to-vacuole targeting pathway, and pexophagy in yeast and mammalian cells. Annu. Rev. Biochem. **69,** 303–342.

Kitamura, S., Shikazono, N., and Tanaka, A. (2004). TRANSPARENT TESTA 19 is involved in the accumulation of both anthocyanins and proanthocyanidins in *Arabidopsis*. Plant J. **37,** 104–114.

Kubo, H., Nozue, M., Kawazaki, K., and Yasuda, H. (1995). Intravacuolar spherical boides in *Polygonum cupsidatum*. Plant Cell Phyisol. **36,** 1453–1458.

Marinova, K., et al. (2007). The *Arabidopsis* MATE transporter TT12 acts as a vacuolar flavonoid/H+-antiporter active in proanthocyanidin-accumulating cells of the seed coat. Plant Cell. **19,** 2023–2038.

Markham, K.R., Gould, K.S., Winefield, C.S., Mitchell, K.A., Bloor, S.J., and Boase, M.R. (2000). Anthocyanic vacuolar inclusions: their nature and significance in flower colouration. Phytochemistry. **55,** 327–336.

Marrs, K.A., Alfenito, M.R., Lloyd, A.M., and Walbot, V. (1995). A glutathione *S*-transferase involved in vacuolar transfer encoded by the maize gene *bronze-2*. Nature. **375,** 397–400.

Marty, F. (1999). Plant vacuoles. Plant Cell. **11,** 587–599.

Moriyasu, Y., and Hillmer, S. (2000). Autophagy and vacuole formation. In Vacuolar Compartments, Robinson, D.G., and Rogers, J.C., eds (Sheffield: Sheffield Academic Press Ltd).

Mueller, L.A., Goodman, C.D., Silady, R.A., and Walbot, V. (2000). AN9, a petunia glutathione *S*-transferase required for anthocyanin sequestration, is a flavonoid-binding protein. Plant Physiol. **123,** 1561–1570.

Murashige, T., and Skoog, F. (1962). A revised medium for rapid growth and bioassays with tobacco tissue cultures. Physiol Plant. **15,** 473–479.

Nair, U., and Klionsky, D.J. (2005). Molecular mechanisms and regulation of specific and nonspecific autophagy pathways in yeast. J. Biol. Chem. **280,** 41785–41788.

Nozue, M., and Yasuda, H. (1985). Occurrence of anthocyanoplasts in cell suspension cultures of sweet potato. Plant Cell Rep. **4,** 252–255.

Nozue, M., et al. (2003). VP24 found in anthocyanic vacuolar inclusions (AVIs) of sweet potato cells is a member of a metalloprotease family. Biochem. Eng. J. **14,** 199–205.

Nozue, M., Nishimura, M., Katou, A., Hattori, C., and Usuda, N. (1993). Characterization of intravacuolar pigmented structures in anthocyanin-containing cells of sweet potato suspension cultures. Plant Cell Physiol. **34,** 803–808.

Nozue, M., Yamada, K., Nakamura, T., Kubo, H., Kondo, M., and Nishimura, M. (1997). Expression of a vacuolar protein (VP24)

in anthocyanin-producing cells of sweet potato in suspension culture. Plant Physiol. **115,** 1065–1072.

Nozzolillo, C., and Ishikura, N. (1988). An investigation of the intracellular site of anthocyanoplasts using isolated protoplasts and vacuoles. Plant Cell Rep. **7,** 389–392.

Pecket, C.R., and Small, C.J. (1980). Occurrence, location and development of anthocyanoplasts. Phytochemistry. **19,** 2571–2576.

Peer, W.A., and Murphy, A.S. (2006). Flavonoids as signal molecules: targets of flavonoid action. In The Science of Flavonoids, Grotewold, E., ed. (New York: Springer Science + Business Media Inc), pp. 239–268.

Phillips, A.R., Suttangkakul, A., and Vierstra, R.D. (2008). The ATG12-conjugating enzyme ATG10 Is essential for autophagic vesicle formation in *Arabidopsis thaliana*. Genetics. **178,** 1339–1353.

Pourcel, L., and Grotewold, E. (2009). Participation of phytochemicals in plant development and growth. In Plant-Derived Natural Products: Synthesis, Function and Application, Osbourn, A.E., and Lanzotti, V., eds (Springer), pp. 269–279.

Poustka, F., et al. (2007). A trafficking pathway for anthocyanins overlaps with the endoplasmic reticulum-to-vacuole protein sorting route in *Arabidopsis* and contributes to the formation of vacuolar inclusions. Plant Physiol. **145,** 1323–1335.

Small, C.J., and Pecket, R.C. (1980). Occurrence, location and development of anthocyanoplasts. Phytochemistry. **19,** 2571–2576.

Small, C.J., and Pecket, R.G. (1982). The ultrastructure of anthocyanoplasts in red cabagge. Planta. **154,** 97–99.

Taylor, L.P., and Grotewold, E. (2005). Flavonoids as developmental regulators. Curr. Opin. Plant. Biol. **8,** 317–323.

Thompson, A.R., and Vierstra, R.D. (2005). Autophagic recycling: lessons from yeast help define the process in plants. Curr. Opin. Plant Biol. **8,** 165–173.

Thompson, A.R., Doelling, J.H., Suttangkakul, A., and Vierstra, R.D. (2005). Autophagic nutrient recycling in *Arabidopsis* directed by the ATG8 and ATG12 conjugation pathways. Plant Physiol. **138,** 2097–2110.

Tohge, T., et al. (2005). Functional genomics by integrated analysis of metabolome and transcriptome of *Arabidopsis* plants over-expressing an MYB transcription factor. Plant J. **42,** 218–235.

Verweij, W., et al. (2008). An H+ P-ATPase on the tonoplast determines vacuolar pH and flower colour. Nat. Cell Biol. **10,** 1456–1462.

Winkel, B.S.J. (2004). Metabolic channeling in plants. Annu. Rev. Plant Biol. **55,** 85–107.

Winkel, B.S.J. (2008). The biosynthesis of flavonoids. In The Science of Flavonoids, Grotewold, E., ed. (New York: Springer Science + Business Media, LLC), pp. 71–95.

Winkel-Shirley, B. (1999). Evidence of enzyme complexes in the phenylpropanoid and flavonoid pathways. Physiol. Plant. **107,** 142–149.

Xu, W., et al. (2000). Detection and characterization of a 36-kDa peptide in C-terminal region of a 24-kDa vacuolar protein (VP24) precursor in anthocyanin-producing sweet potato cells in suspension culture. Plant Sci. **160,** 121–128.

Xu, W., Shioiri, H., Kojima, M., and Nozue, M. (2001). Primary structure and expression of a 24-kD vacuolar protein (VP24) precursor in anthocyanin-producing cells of sweet potato in suspension culture. Plant Physiol. **125,** 447–455.

Zhang, H., Wang, L., Deroles, S., Bennett, R., and Davies, K. (2006). New insight into the structures and formation of anthocyanic vacuolar inclusions in flower petals. BMC Plant Biol. **6,** 29.

Zouhar, J., Rojo, E., and Bassham, D.C. (2009). AtVPS45 is a positive regulator of the SYP41/SYP61/VTI12 SNARE complex involved in trafficking of vacuolar cargo. Plant Physiol., in press.